

In-Situ Growth of Graphene on Hexagonal Boron Nitride for Electronic Transport Applications

Hadi Arjmandi-Tash,^{*a} Zheng (Vitto) Han,^b and Vincent Bouchiat^c

Transferring graphene flakes onto hexagonal boron nitride (h-BN) has been the most popular approach for the fabrication of graphene/h-BN heterostructures so far. The orientation between graphene and h-BN lattices, however, are not controllable and the h-BN/graphene interfaces are prone to be contaminated during this elaborate process. Direct synthesis of graphene on h-BN is an alternative and rapidly growing approach. Synthesized graphene via such approaches is personally tailored to conform to each specific h-BN flakes, hence the limitations of conventional fabrication approaches are overcome. Reported processes paved the initial steps to improve the scalability of the device fabrication for industrial applications. Reviewing the developments in the field, from the birth point to the current status is the focus of this letter. We show how the field has been developed to overcome the existing challenges one after the other and discuss where the field is heading to.

Introduction

Electronic mobility in supported graphene is highly limited by the roughness and the charged impurities on the surface of the substrate^{1,2,3}. Inserting a thick ($\gtrsim 10\text{nm}$) buffer layer of hexagonal boron nitride – with atomically flat and neutral surface – in between graphene and the supporting substrate helps to overcome those limitations. Heterostructure of graphene on multilayer h-BN flakes was first successfully realized and studied by C. Dean et al⁴; their device exhibited charge carrier mobilities as high as $140,000\text{ cm}^2/\text{Vs}$ which was not reachable on supported devices by that time. Next work from the same group⁵ also confirmed the advantages of h-BN as a mattress for CVD graphene. Lately by sandwiching graphene between two h-BN layers, very long

mean free paths and ballistic transport was reported even at room temperature^{6,7}. Its dielectric nature and lattice parameter – which is close to that of graphene – are the other remarkable properties of h-BN as a mattress for graphene.

In all these reports, chemical vapor deposition (CVD) or exfoliated graphene is first isolated on an intermediate substrate and then transferred onto the h-BN flakes. The process is of remarkable disadvantages: *i)* contaminating the surface of h-BN and graphene is highly possible during this process as air or water molecules might be trapped at the interface. *ii)* graphene can be damaged or wrinkled and *iii)* the process does not provide any control over the relative orientation of graphene and h-BN: the random orientation of the lattices may lead to irreproducible results. *iv)* Macroscopic alignment of microscale graphene on h-BN flakes is another issue which is time-consuming and troublesome in practice.

Transfer-free, direct growth of graphene on h-BN techniques offer solutions to overcome the limitations listed

^{*a} Leiden Institute of Chemistry, Faculty of Science, Leiden University, Leiden, Netherlands.
E-mail: h.arjmandi.tash@lic.leidenuniv.nl

^b Institute of Metal Research Chinese Academy of Sciences, Shenyang, Liaoning, 110016, China

^c University of Grenoble Alpes, CNRS, Institut Néel, F-38000 Grenoble, France.

above. Particularly, in such techniques the graphene/h-BN interface is realized *in-situ* and thus no external contaminant may get trapped in between.

In this letter, we review the progress of the techniques to grow graphene on thick h-BN flakes. Standard CVD of graphene benefits from the presence of a catalyst (e.g. copper) as the promoter of the growth; the absence of such a catalyst hinders direct growing of graphene on h-BN. We discuss how different approaches tackled this limitation. Different aspects of such growth methods are reviewed here. Note that there are some methods developed for growing both graphene and mono- (few-) layer h-BN together to make thin ($\lesssim 10\text{nm}$) graphene/h-BN stacks or patchworks^{8,9,10,11}; Interestingly, the growth of the first sample of this type was reported even before the first realization of graphene by exfoliation¹². Thickness of h-BN layers achieved in such approaches, however, are not enough to smoothen the roughness of underlying substrates and diminish the effect of the random potentials resting on the wafer; such approaches are out of the scope of this letter then.

1 Yield issues in *in-situ* growth of graphene

Chemical growth of graphene relies based on the decomposing carbon-rich precursor molecules (e.g. methane) at the presence of a catalyst. The elevated temperature of the growth chamber provides enough energy for the reoultant carbon atoms to get mobilized and reach and bind the other carbon atoms and form a graphene layer. Indeed the presence of the catalyst plays a vital role to speed-up the growth: skipping the catalyst is a major limitation for the growth of graphene on arbitrary (*i.e.* non-catalyst) substrates such as on h-BN.

The first paper about directly growing CVD graphene on h-BN was submitted for publication just four months after the first realization of the graphene/h-BN stacking⁴. The rapid inception implies the importance of the *in-situ* growth approaches in the first place. Published by Ding *et al*¹³, this paper confirmed the possibility of chemically growing few-

layer graphene on h-BN powders. The importance of catalyst was, however, overlooked: no remarkable arrangement was considered to compensate its absence. The size of the graphene domains remained unclear; even-though as a normal CVD process with very short growth time (compared to the later reports) was used, domains larger than few nanometers are hardly expected. Figure 1-a and b shows some of the results. Lately and as the field started developing, few approaches have been introduced to overcome the absence of the catalyst.

1.1 Elongated growth

Elongating the growth course is the simplest approach to compensate the absence of the catalyst. Son *et al*¹⁴ mechanically exfoliated h-BN flakes on a silicon wafer and grew graphene in an atmospheric pressure CVD chamber. Different growth temperatures ranging between 900°C to 1000°C with a similar growth duration of 2 hours were tested. Domains of $\sim 100\text{nm}$ in diameter achieved. They reported a direct trend of increasing the density of the graphene pads upon increasing the growth temperature (Figure 1-c and d). The grown graphene flakes were of rounded shapes with the thicknesses of the order of 0.5 nm. AFM, Raman and XPS analysis have been performed to confirm the growth and characterize the graphene.

The approach was followed later by Tang *et al*¹⁵. Like the Son's experiment, graphene was grown on hexagonal boron nitride flakes exfoliated on silicon wafer, albeit through a low pressure CVD process. They noticed that screw dislocations on the flakes are favorable nucleation sites. The slow growth rate due to the missing of the catalyst was very evident in the results reported; a growth duration of 6 hours only led to the formation of graphene grains of maximum 270 nm in diameter (Figure 1-e to g). The graphene domains were mostly single layer.

Elongating the growth – although is simple – is of certain drawbacks: The reported graphene domains – even after several hours of growth – could hardly reach few hundreds

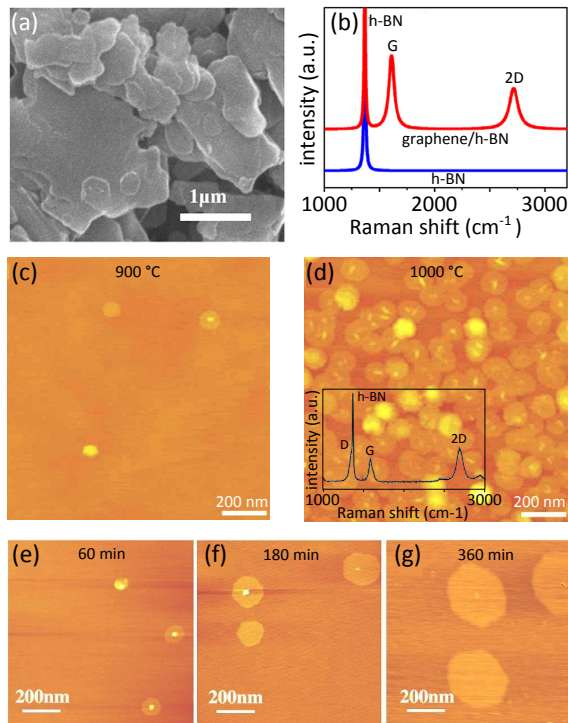


Fig. 1 Early reports on the direct growth of graphene on thick h-BN flakes
a) and (b) Results of Ding *et al*: Graphene was grown on h-BN powders through a CVD process. The Raman spectra on (b) are taken from bare h-BN powder and after the growth. Reprinted from ¹³, Copyright (2011), with permission from Elsevier.
c) and (d) Results of Son *et al*: The effect of the growth temperature on the density of the obtained flakes was reported as AFM mappings in this work. The density raised a lot as the temperature increased from 900 °C to 1000 °C. This growth lasts for 2 hours. The inset in (d) shows an example of the Raman spectrum reported on this sample. Adapted from ¹⁴ with permission of The Royal Society of Chemistry.
e), (f) and (g) Results of Tang *et al*: AFM measurements shown in these figures were performed on the samples with 1, 3 and 6 hours of growth. Reprinted from ¹⁵, Copyright (2012), with permission from Elsevier.

of nanometers and are incompatible with typical device fabrication processes. The long operation time and high energy consumption are unfavorable for industrial applications.

1.2 Optimized growth parameters

Fine-tuning the growth parameters is a wiser approach to improve the yield. Mishra *et al*¹⁶ showed that in a typical CVD process, increasing the partial pressure of hydrogen and elevating the growth temperature can achieve an improved growth rate of up to 100 nm/min (to be compared with 5 nm/min with standard CVD growth parameters¹⁷) (Figure 2-a). They systematically investigated the effect of the partial pressure of hydrogen on the crystallinity of the grown graphene domains: Low partial pressure of

hydrogen (H_2 to CH_4 ratio of 1:1) mainly achieved circular poly-crystalline grains. Increasing the partial pressure of hydrogen (H_2 to CH_4 ratio of 30:1), however, led to the formation of van der Waals epitaxy (discussed in section 2) with aligned hexagonal grains. Indeed reducing the density of nucleation centers via hydrogen etching plays a vital role in reported results.

1.3 Plasma-enhanced chemical vapor deposition

Inspired by earlier works on the growth of graphene on non-catalyst substrates^{18 19}, Yang *et al* employed remote plasma-enhanced chemical vapor deposition (RPE-CVD) technique to grow graphene on exfoliated h-BN flakes²⁰. Here a remote plasma source decomposes methane molecules into various reactive radicals prior reaching the substrate; hence catalyst can be omitted. The approach provides enough control over the number of layers and uniformity of graphene. In principal, the size of the graphene is only limited by the size of underlying h-BN flakes. Growth temperature controls both the epitaxy and the rate of the growth: Even-though increasing the growth temperature improves the growth rate, population of nucleation centers also increases at the same time which may lead to three-dimensional – instead of layer by layer – growth and suppress the epitaxy. The growth temperature of ~500 °C was the best compromise between epitaxy and growth rate. In this condition, several growth periods, each of two to three hours are still required to obtain the desired graphene sizes.

1.4 Gaseous catalyst

While the presence of the h-BN as a background substrate does not leave any room for a solid catalyst, Tang *et al*¹⁷ used gaseous silane (SiH_4) and germane (GeH_4) catalysts to boost the growth. At a temperature of 1280 °C, the growth rate reached 50 nm/min and 400 nm/min, respectively in the presence of germane and silane: the yield was highly improved comparing to the recorded 5 nm/min in the absence of any catalyst. They noticed that elevating the growth temperature upto 1350 °C further accelerate the growth to reach

$\sim 1 \mu\text{m}/\text{min}$ (Figure 2-b). Importantly, the Auger electron spectroscopy of the domains did not exhibit any trace of silicon or germanium in the grown graphene crystal. Apparently, those atoms only stick to the edge of the graphene domains and lower the reaction barrier for carbon precursors to form the honeycomb lattice during the growth (Figure 2-c). AFM analyses confirmed that more than 93% of the graphene domains are well oriented with respect to the background lattice of h-BN.

1.5 Proximity-driven overgrowth

A new approach in the growth of graphene on non-catalyst materials such as h-BN was introduced by our group recently²¹. Unlike the previous approaches, the growth is performed on h-BN flakes which are pre-exfoliated on the copper foil (Figure 2-d). Hence, the carbon-rich precursors still have access to catalyst, albeit indirectly. The growth rate of graphene on h-BN was improved dramatically: a full coverage of graphene on millimeter sized h-BN flake is achievable in the same rate of graphene on surrounding copper foil (Figure 2-e). The obtained devices exhibited charge carrier mobilities of $20,000 \text{ cm}^2/\text{Vs}$ and very neutral graphene-h-BN interfaces.

2 Growth mechanism

In fabricating heterostructures by depositing a material on a substrate at least two mechanisms are considerable: In materials with terminating layers full of dangling bonds, atoms in one material can establish covalent bounds only to the atoms of very similar lattice; indeed the covalent bonds are very sensitive to the length and the angle between the atoms. This is an important hindrance in epitaxial growth between materials with different lattice parameters. Figure 3-a schematically illustrates this mechanism. The situation is very different in between two materials with perfect terminating surfaces and no dangling bonds (Figure 3-b). Here, the absence of the dangling bonds can lead to the formation of very sharp interfaces with small amount of defects. This growth mechanism is referred to as *van der Waals*

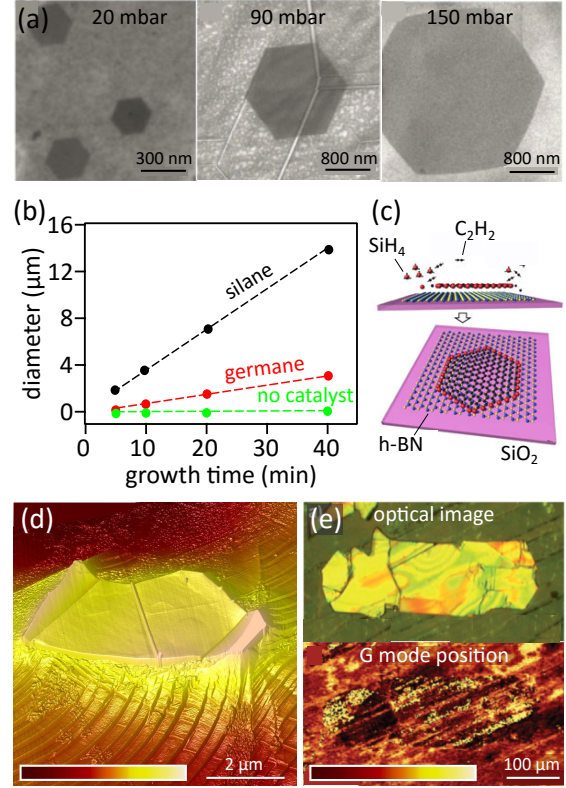


Fig. 2 Various approaches to improve the growth rate
a) Effect of increasing the growth pressure on the grain size: SEM images showing graphene grains synthesized on h-BN flakes at 1150°C under various chamber pressures. Reprinted from¹⁶, Copyright (2016), with permission from Elsevier.
b and c) Gaseous phase catalyst to improve the growth rate: b) comparison of the experimentally measured grain size of graphene flakes grown at 1280°C with and without gaseous catalysts. c) Schematic illustration showing the mechanism of growing monolayer graphene onto h-BN: silicon atoms (shown as red color spheres) achieved from the decomposition of SiH_4 bind to the edge of the graphene and boost the growth. Reprinted with adaptations from¹⁷.
d and e) Proximity driven over growth of graphene onto h-BN flakes pre-exfoliated on the copper foil: d) AFM mapping showing an h-BN flake (covered with graphene) on the copper foil at the end of the growth course. The color code shows the height, ranging between 0 nm and 500 nm . e) Optical image (top) and Raman G mode position mapping (bottom) of a millimeter scale h-BN flake on the copper foil, fully covered by graphene. The color code shows the Raman frequency ranging between 1584 cm^{-1} and 1600 cm^{-1} . Reprinted with adaptations from²¹.

epitaxy and can be realized even in the presence of large lattice mismatches^{22 23}. As graphene and h-BN are both free from dangling bonds, van der Waals epitaxy is normally the governing growth mechanism.

Garcia *et al*²⁴ first reported van der Waals epitaxy in *in-situ* growing graphene on h-BN. Unlike the previous experiments, graphene was grown by molecular beam epitaxy (MBE) using solid carbon sources. Combined Raman and AFM analysis revealed that the growth is independent of the flux of carbon atoms; instead, carbon atoms deposited on the surface, migrate freely and accumulate in selective spots on the h-BN surface (Figure 3-b and c). This observation pointed out that the carbon atoms are of very high mobilities on the neutral h-BN, confirming that van der Waals epitaxy was achieved. Recently, van der Waals epitaxy was reported in CVD growth of graphene on h-BN also¹⁶.

A separate but complementary growth mechanism involves extending graphene – already nucleated on the copper foil – onto nearby h-BN flakes. This mechanism was first observed in graphene grown on few-layer chemically grown h-BN sheets¹¹; our recent work²¹, however, confirmed that the thickness of the h-BN is not any limitation as graphene can overgrow on hundreds-of-nanometers-thick h-BN flakes, mechanically pre-exfoliated on the copper foil. Inset to Figure 3-d explains our hypothesized model for this growth. Precursors are cracked on the copper foil. The achieved carbon radicals move randomly in different directions and are energetic enough to continuously jump over the h-BN flake and bond as-growing graphene. The presence of the copper catalyst and high mobility of carbon atoms – as a result of the van der Waals epitaxy – guarantees high growth rate atop h-BN flakes. The main panel of Figure 3-d shows SEM image of a h-BN flake covered with graphene.

3 Epitaxial Growth

Once two similar patterns of crystalline lattices (*e.g.* graphene and h-BN lattices) are superimposed with a small displacement or rotation in between, a secondary pattern known as moiré generates^{25 26}. Moiré superlattice poten-

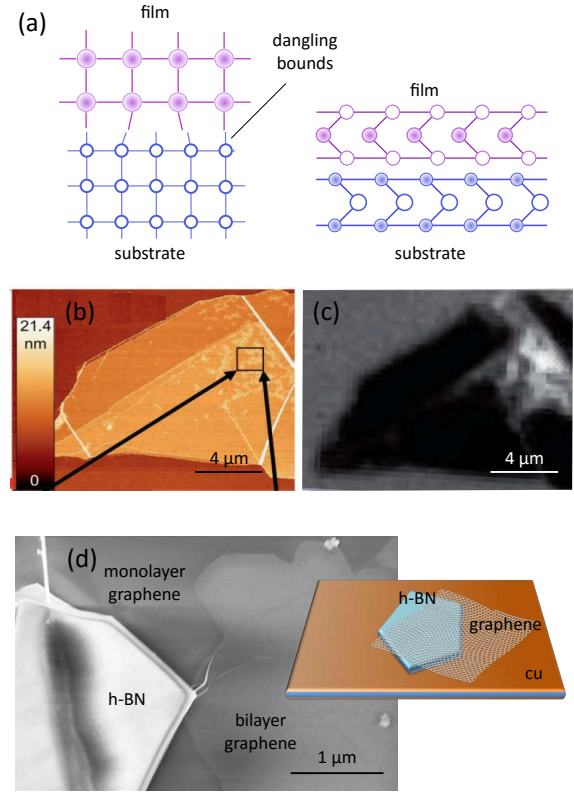


Fig. 3 Known mechanisms governing the growth of graphene on h-BN flakes

a) Comparison of the epitaxial growth in between materials with (left) and without (right) dangling bonds, the latter has been dubbed *van der Waals epitaxy*; in both cases the atoms, corresponding to the substrate and to the deposited film are shown in blue and pink respectively.

b) AFM and c) Raman (intensity of 2D peak of graphene) mapping of a h-BN flake with deposited graphene via molecular beam epitaxy; the mappings show that carbon atoms are freely migrated and accumulated in some preferential spots on the surface of h-BN. Reprinted from²⁴, Copyright (2012), with permission from Elsevier.

d) Schematic representation of the mechanism (inset) and SEM image of graphene (both mono- and bi-layer) nucleated on the copper foil and extended over the h-BN flake via proximity driven growth.

tial affects the propagation of charge carriers in graphene by inducing new Dirac points, known as *satellite Dirac points* (SDPs) in the band structure of graphene. The energy of SDPs (E_{SDP}) depends on the wave vector of the superlattice (λ_{SL}) which itself is a function of the misorientation angle (Φ) between the lattices:²⁷

$$E_{SDP} = \pm \frac{\hbar v_F |\vec{G}|}{2} = \pm \frac{2\pi\hbar v_F}{\sqrt{3}\lambda_{SL}}, \text{ where:}$$

$$\lambda_{SL} = \frac{(1+\delta)a}{\sqrt{2(1+\delta)(1-\cos\Phi)+\delta^2}}$$

In this relation, \vec{G} represents the reciprocal superlattice vector and $v_F \approx 10^6$ m/s is the Fermi velocity of quasiparticles in graphene. Additionally, $a = 2.46$ and $\delta = 1.8\%$ are the

lattice parameter of graphene and the mismatch between graphene and h-BN lattices, respectively.

Controlling and minimizing the misorientation angle in graphene/h-BN heterostructures is of great importance to lower structural uncertainties. Indeed traditional method of transferring exfoliated graphene on h-BN leads a random orientation of the lattices. Although recent progresses in the field revealed that post-treatment of the samples at elevated temperatures can drive graphene to rotate and follow h-BN lattices^{28,29}, such approaches are more efficient in sub-micrometer flakes. *In-situ* growing graphene on h-BN, however, is of proven capabilities to control Φ in much larger samples.

Yang *et al* utilized plasma-enhanced CVD technique to grow graphene on mechanically exfoliated h-BN flakes²⁰. Large area, epitaxial and single crystal graphene domains directly grown on the h-BN flakes were obtained. Breaking down the methane molecules with a remote plasma source eliminated the need for a catalyst and enhanced the growth rate and the domains size. The cleanness of the flakes was high enough that they manage to observe the moiré pattern associated to superposition of graphene and h-BN crystals by AFM analysis (Figure 4-a,b). This analysis showed that graphene's lattice follows the orientation of the underlying h-BN. The size of the graphene was limited by the size of the h-BN flake, large enough to fabricate devices for transport experiments. The signature of the superposition of the lattices as extra Dirac points in the resistivity and quantum Hall effect measurements revealed at low temperatures (Figure 4-c,d).

We note that similar alignment was reported later by Tang *et al*^{30,17} (Figure 4-e,f) and Mishra *et al*¹⁶.

4 Discussion

Table 1 summarizes the important reports of *in-situ* growing graphene on thick (\gg monolayer) h-BN flakes in a chronological order. Chemical vapor deposition (including its derivatives) using methane precursor has been the most frequently employed method. Such reports demonstrated

the growth in a wide temperature range.

The size of the resultant graphene samples and growth rate have been improved gradually over the last years. Similar improvements in controlling the thickness (number of layers) of graphene is also detectable. While the orientation of graphene in early reports were unclear, recent works reported a trend in graphene/h-BN lattice alignment. The best mobility reported for *in-situ* grown samples is still much inferior than what is achieved in transfer-fabricated samples, even with CVD graphene⁵ which points out the affect of crystalline defects. Indeed the techniques employed to compensate the lack of catalysts – even-though successful to preserve the growth rate – yet failed to yield crystalline qualities comparable to that of graphene grown on a catalyst.

5 Conclusion and perspective

In-situ growth of graphene on h-BN provides the possibility for achieving hetero-structures with clean interfaces. The risk of damaging graphene during transfer-fabrication is eliminated. Some growth approaches can even yield to the alignment of graphene with respect to the underlying h-BN lattice. While early attempts suffer from low growth rate as a result of the skipping of the catalyst, the new development in which the catalyst material indirectly promotes the growth guaranteed full coverage of millimeterscale h-BN flakes with a rate identical on the catalyst.

The electronic transport properties of graphene achieved by *in-situ* growth approaches are still inferior than the devices achieved in transfer-fabrication methods. Indeed crystalline defects serving as charge carrier scattering centers are abundant; certain measures have to be taken to improve the crystalline order of graphene in the future.

Sandwiching graphene in between two h-BN flakes provides the best device quality; no *in-situ* growth method has yet succeeded to yield such structures. Additionally, direct growth of van der Waals hetero-structures with multiple two-dimensional materials is on the perspective. The choice of CVD is based on the qualification of the methods in

Table 1 Summary of the reports of *in-situ*growing graphene on thick h-BN flakes, in chronological order

report	process	precursor	temperature	duration	size	thickness	orientated [‡]	mobility
Ding ¹³	CVD	CH ₄ (50-90 sccm)	1000°C	3-8 min	not reported	> 6 L	not clear	not reported
Son ¹⁴	CVD	CH ₄ (30-50 sccm)	900-1000°C	2 hrs	100 nm	≈ 0.5 nm	not clear	not reported
Tang ¹⁵	CVD	CH ₄ (5 sccm)	1200°C	1-6 hrs	<270 nm	ML	not clear	not reported
Garcia ²⁴	MBE	solid carbon	600-930°C	40.6 min	nm-scale	ML	not clear	not reported
Yang ²⁰	PECVD	CH ₄ [†]	≈ 500°C	≥ 3 hrs	μm-scale	ML& BL	yes	~ 5,000 cm ² /Vs (at 1.5 K)
Tang ³⁰	CVD	CH ₄ (5 sccm)	1200°C	1-5 hrs	μm-scale	ML& BL	yes	20,000 cm ² /Vs (at 300 K)
Tang ¹⁷	CVD	C ₂ H ₂ [†]	1280-1350°C	5-40 min	μm-scale	ML	yes	20,000 cm ² /Vs (at 300 K)
Mishra ¹⁶	cold-wall CVD	CH ₄ [†]	1000-1150°C	30 min	μm-scale	ML	yes	not reported
Arjmandi-Tash ²¹	CVD	CH ₄ (5 sccm)	1050°C	90 s	mm-scale	ML	not clear	20,000 cm ² /Vs (at 80 K)

ML: monolayer, BL: bilayer

[‡] if graphene follows the orientation of underlying h-BN

[†] The flow rate of the precursor was not reported in this work.

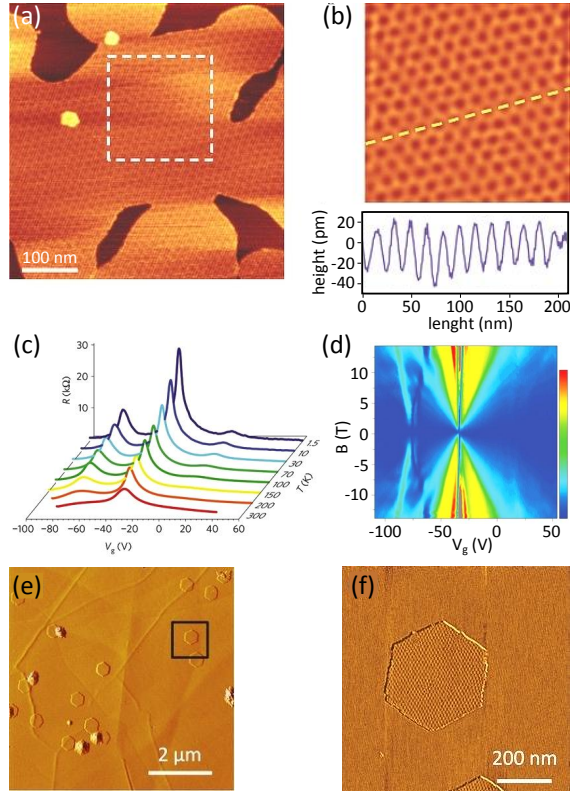


Fig. 4 Crystalline biased growth of graphene on h-BN

a) Moiré pattern due to the superposition of the graphene and h-BN lattices, b) Filtered inverse fast Fourier transform of the pattern which is visible in the dashed square in a, height profile along the dashed line is shown in the lower part. The periodicity of the oscillations can be used to calculate the rotation angle between the lattices. Reprinted by permission from Macmillan Publishers Ltd: Nature Materials²⁰, copyright (2013). c) Gate dependence of the resistivity measured at different temperatures: satellite peaks shown at the left and right side of the Dirac point are due to the formation of the superlattice. d) This effect also shows up as the pattern at the left side of the fan diagram of the R_{xx} in the quantum hall measurement. Reprinted by permission from Macmillan Publishers Ltd: Nature Materials²⁰, copyright (2013). e) Topography of the small graphene flakes and (f) moiré pattern associated to graphene/h-BN superposition. Reprinted with adaptations from³⁰. The mappings shown in a, b, e and f are done with atomic force microscopy.

growing graphene on copper. Certain efforts, however, have

to be made to evaluate the efficiency of other approaches (e.g. bottom-up synthesis using polycyclic aromatic hydrocarbons) in growing graphene on h-BN.

References

- 1 E. Hwang, S. Adam and S. Sarma, *Phys. Rev. Lett.*, 2007, **98**, 2–5.
- 2 X. Du, I. Skachko, A. Barker and E. Y. Andrei, *Nat. Nanotechnol.*, 2008, **3**, 491–5.
- 3 A. S. Mayorov, D. C. Elias, I. S. Mukhin, S. V. Morozov, L. a. Ponomarenko, K. S. Novoselov, a. K. Geim and R. V. Gorbachev, *Nano Lett.*, 2012, **12**, 4629–34.
- 4 C. R. Dean, a. F. Young, I. Meric, C. Lee, L. Wang, S. Sorgenfrei, K. Watanabe, T. Taniguchi, P. Kim, K. L. Shepard and J. Hone, *Nat. Nanotechnol.*, 2010, **5**, 722–6.
- 5 N. Petrone, C. R. Dean, I. Meric, A. M. van der Zande, P. Y. Huang, L. Wang, D. Muller, K. L. Shepard and J. Hone, *Nano Lett.*, 2012, **12**, 2751–6.
- 6 A. S. Mayorov, R. V. Gorbachev, S. V. Morozov, L. Britnell, R. Jalil, L. a. Ponomarenko, P. Blake, K. S. Novoselov, K. Watanabe, T. Taniguchi and a. K. Geim, *Nano Lett.*, 2011, **11**, 2396–9.
- 7 L. Wang, I. Meric, P. Y. Huang, Q. Gao, Y. Gao, H. Tran, T. Taniguchi, K. Watanabe, L. M. Campos, D. a. Muller, J. Guo, P. Kim, J. Hone, K. L. Shepard and C. R. Dean, *Science*, 2013, **342**, 614–7.
- 8 M. Wang, S. K. Jang, W.-J. Jang, M. Kim, S.-Y. Park, S.-

- W. Kim, S.-J. Kahng, J.-Y. Choi, R. S. Ruoff, Y. J. Song and S. Lee, *Adv. Mater.*, 2013, **25**, 2746–52.
- 9 S. Roth, F. Matsui, T. Greber and J. Osterwalder, *Nano Lett.*, 2013, **13**, 2668–75.
- 10 Z. Liu, L. Song, S. Zhao, J. Huang, L. Ma, J. Zhang, J. Lou and P. M. Ajayan, *Nano Lett.*, 2011, **11**, 2032–7.
- 11 S. M. Kim, A. Hsu, P. T. Araujo, Y.-H. Lee, T. Palacios, M. Dresselhaus, J.-C. Idrobo, K. K. Kim and J. Kong, *Nano Lett.*, 2013, **13**, 933–41.
- 12 C. Oshima, A. Itoh, E. Rokuta, T. Tanaka, K. Yamashita and T. Sakurai, *Solid State Commun.*, 2000, **116**, 37–40.
- 13 X. Ding, G. Ding, X. Xie, F. Huang and M. Jiang, *Carbon N. Y.*, 2011, **49**, 2522–2525.
- 14 M. Son, H. Lim, M. Hong and H. C. Choi, *Nanoscale*, 2011, **3**, 3089–93.
- 15 S. Tang, G. Ding, X. Xie, J. Chen, C. Wang, X. Ding, F. Huang, W. Lu and M. Jiang, *Carbon N. Y.*, 2012, **50**, 329–331.
- 16 N. Mishra, V. Miseikis, D. Convertino, M. Gemmi, V. Piazza and C. Coletti, *Carbon N. Y.*, 2016, **96**, 497–502.
- 17 S. Tang, H. Wang, H. S. Wang, Q. Sun, X. Zhang, C. Cong, H. Xie, X. Liu, X. Zhou, F. Huang, X. Chen, T. Yu, F. Ding, X. Xie and M. Jiang, *Nat. Commun.*, 2015, **6**, 6499.
- 18 L. Zhang, Z. Shi, Y. Wang, R. Yang, D. Shi and G. Zhang, *Nano Res.*, 2011, **4**, 315–321.
- 19 L. Zhang, Z. Shi, D. Liu, R. Yang, D. Shi and G. Zhang, *Nano Res.*, 2012, **5**, 258–264.
- 20 W. Yang, G. Chen, Z. Shi, C.-c. Liu, L. Zhang, G. Xie, M. Cheng, D. Wang, R. Yang, D. Shi, K. Watanabe and T. Taniguchi, *Nat. Mater.*, 2013, 792–797.
- 21 H. Arjmandi-Tash, D. Kalita, Z. Han, R. Othmen, C. Berne, J. Landers, K. Watanabe, T. Taniguchi, L. Marty, J. Coraux, N. Bendiab and V. Bouchiat, *arXiv submit/1772663*, 2017.
- 22 K. Ueno, K. Sasaki, N. Takeda, K. Saiki and A. Koma, *Appl. Phys. Lett.*, 1997, **70**, 1104.
- 23 K. Sasaki, K. Ueno and A. Koma, *Jpn. J. Appl. Phys.*, 1997, **36**, 4061–4064.
- 24 J. M. Garcia, U. Wurstbauer, A. Levy, L. N. Pfeiffer, A. Pinczuk, A. S. Plaut, L. Wang, C. R. Dean, R. Buizza, A. M. Van Der Zande, J. Hone, K. Watanabe and T. Taniguchi, *Solid State Commun.*, 2012, **152**, 975–978.
- 25 J. Xue, J. Sanchez-yamagishi, D. Bulmash, P. Jacquod, A. Deshpande, K. Watanabe, T. Taniguchi, P. Jarillo-herrero and B. J. Leroy, *Nat. Mater.*, 2011, **10**, 282–5.
- 26 R. Decker, Y. Wang, V. W. Brar, W. Regan, H.-z. Tsai, Q. Wu, W. Gannett, A. Zettl and M. F. Crommie, *Nano Lett.*, 2011, **11**, 2291–2295.
- 27 M. Yankowitz, J. Xue, D. Cormode, J. D. Sanchez-Yamagishi, K. Watanabe, T. Taniguchi, P. Jarillo-Herrero, P. Jacquod and B. J. LeRoy, *Nat. Phys.*, 2012, **8**, 382–386.
- 28 D. Wang, G. Chen, C. Li, M. Cheng, W. Yang, S. Wu, G. Xie, J. Zhang, J. Zhao, X. Lu, P. Chen, G. Wang, J. Meng, J. Tang, R. Yang, C. He, D. Liu, D. Shi, K. Watanabe, T. Taniguchi, J. Feng, Y. Zhang and G. Zhang, *Phys. Rev. Lett.*, 2016, **116**, 1–6.
- 29 C. R. Woods, F. Withers, M. J. Zhu, Y. Cao, G. Yu, A. Kozikov, M. Ben Shalom, S. V. Morozov, M. M. van Wijk, A. Fasolino, M. I. Katsnelson, K. Watanabe, T. Taniguchi, A. K. Geim, A. Mishchenko and K. S. Novoselov, *Nat. Commun.*, 2016, **7**, 10800.
- 30 S. Tang, H. Wang, Y. Zhang, A. Li, H. Xie, X. Liu, L. Liu, T. Li, F. Huang, X. Xie and M. Jiang, *Sci. Rep.*, 2013, **3**, 2666.